Colloid Polym Sci (2005) 284: 160–166
DOI 10.1007/s00396-005-1352-z

ORIGINAL CONTRIBUTION

Horst Kresse
Jürgen Lindau
Siegmar Diele
Julia Salfetnikova
Anton Hauser
Erika Hempel

Sn-containing liquid crystalline side group homopolymers with two glass transitions

Received: 4 April 2005
Accepted: 10 May 2005
Published online: 8 July 2005

H. Kresse (✉) · J. Lindau · S. Diele
J. Salfetnikova · A. Hauser
Fachbereich Chemie,
Institut für Physikalische Chemie,
Martin-Luther-Universität Halle,
Mühlpforte 1, 06108 Halle, Germany
E-mail: horst.kresse@chemie.uni-halle.de
Tel.: +49-345-5525846
Fax: +49-345-5527157

E. Hempel
Fachbereich Physik,
Martin-Luther-Universität Halle,
Hoher Weg 8, 06099 Halle, Germany

Abstract Three homologous tin-containing homopolymers with a terminal CN-dipole in the side group have been synthesized and characterized by dynamical calorimetry, polarization microscopy, X-ray and dielectric methods. AFM was used to evaluate the texture at room temperature. Four different phase transitions were detected by DSC. The high temperature phases were identified by polarization microscopy as SmA and SmC. AFM-measurements show focal-conic domains at room temperature and confirm so the smectic nature of all phases. X-ray measurements on nonoriented samples give hints to a phase segregation on nanometer scale. Dielectric investigation and temperature-modulated DSC (TMDSC) confirm clearly phase separation by appearance of two glass transitions related to the liquid order of the main chains and the liquid crystalline of the side groups.

Keywords Liquid crystalline homopolymers · Phase separation · Two glass transitions

Introduction

If molecules of two nonmiscible liquids are connected via a chemical bond, phase separation on a small length scale can be expected. This concept is widely used for the synthesis of thermotropic and lyotropic materials forming liquid crystalline mesophases [1–3] and was also extended to side group polymers. In the latter case, an experimental evidence for the phase segregation between the main chains and the side groups was given by structure investigations [4–8].

Surprisingly, on newly synthesized tin-containing liquid crystalline side group homopolymers with the strong $-NO_2$ dipole in the terminal position also phase segregation was observed although both parts, the main chain and the side group, are miscible. The Sn-atoms were introduced in the main chain in order to make this part better visible in X-ray investigations. In this way, the phase separation could be better observed [9]. The appearance of two glass transitions related to the separate freezing process of the main chains and of the side groups, respectively, could be proven recently also by dynamical methods [10, 11].

In order to check whether this effect is a singularity for the class of nitro-samples or probably a typical effect of many side group homopolymers three tin-containing polymers with a terminal CN-dipole in the side group were synthesized and characterized by X-ray and dynamical methods. Thereby, it is very important to combine different dynamical methods (see also [12, 13]).

Experimental part

Samples

The following three tin-containing homopolymers **PY** with the spacer length $y = 6$, 8, and 10 were synthesized according to the published synthetic route [9].

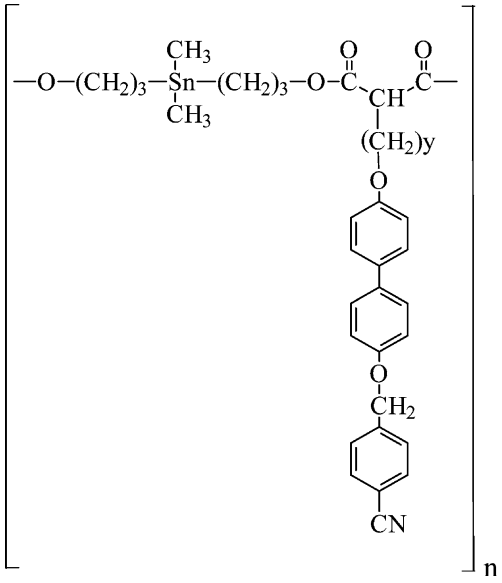

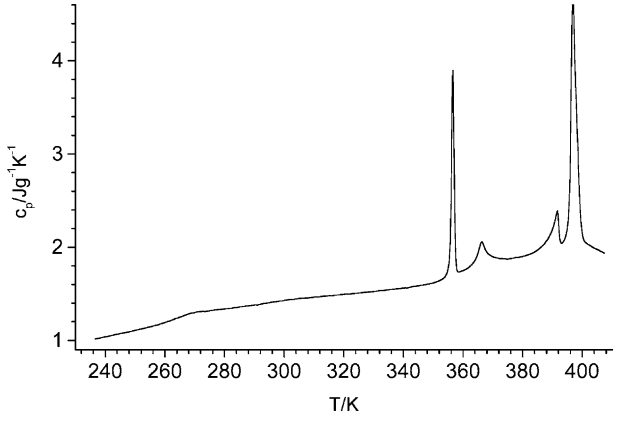

Fig. 1 DSC trace of sample **P8** (heating rate: 10 $Kmin^{-1}$)

Table 1 Phase transition temperatures of the samples in *K*

Sample	I		S_1		S_2		S_3		S_4
P6	●	395	●	392	●	367	●	355	●
P8	●	399	●	394	●	368	●	357	●
P10	●	405	●	398	●	370	●	360	●

A mean degree of polymerization of about 25 was obtained. Detailed information about the analytical data are given in the supplement. The DSC-trace of **P8** in Fig. 1 shows small transition peaks with a half width of 3 K (heating) and 1.5 K (cooling) pointing to a small distribution of the molecular mass. The smectic phases are marked S_4, S_3, S_2 and S_1. Phase transition temperatures calculated from the maximum of DSC traces obtained during cooling are given in Table 1. Glass transitions are not considered.

For classification of the phases, the samples were cooled during the I/S_1 transition with a rate of 1 Kh^{-1} in order to obtain a good texture. Thus, the high temperature phases were identified by polarization microscopy as $S_1 = S_A$ and $S_2 = S_C$. The two low temperature phases could not be classified in this way.

X-ray measurements

X-ray investigations were performed on the nonoriented samples using the Guinier-method [14]. All attempts to orient the sample failed. The powder-like pattern display the first- and second-order of the layer reflection ($d = 4.32$ nm), which is temperature independent. Figure 2a and b show as example the scattered intensity of **P10** in the wide-angle region in the S_3 and S_4 phases, respectively. The X-ray pattern of the homologous **P8** and **P6** qualitatively agree with that of **P10**.

Different temperatures were chosen in order to demonstrate the clear change of the pattern in the wide-angle region which appears at the S_4/S_3 transition. The X-ray data can be summarized to: In the S_4 phase, the two scattering-maxima (related to $d_1 = 0.52$ nm and $d_2 = 0.47$ nm) and an additional sharp wide angle reflection at $d_3 = 0.39$ nm can be seen. The d_3 value is found in systems in which aromatic rings are laterally packed. The given d_2 value is known for disordered aliphatic chains. In the S_3 phase, the reflection with the period d_3 disappears and the second scattering maximum is broadened and shifted to a value known for liquid-like order of mesogens in SmA or SmC phases.Two scattering-maxima prove the existence of disordered main chains as well as of disordered side groups. These results give the first hint to a phase segregation on very small length-scale. This segregation of disordered parts is present in the low temperature phase S_4, too. The origin of the reflection d_3 is not clear, yet. Such scattering is found in discotic systems in which it indicates the lateral distance of the packed aromatic rings. An analogous situation in rod-like mesogens (the side-group in our compounds) is not described up to now.

AFM investigations

AFM measurements were performed using the TMX 1010 Scanning Probe Microscope of TopoMetrix at room temperature and under ambient conditions. The images were obtained by the noncontact method (cantilever resonance frequency: 161 kHz). At first, the sample was filled in a 10-μm sandwich cell consisting of glass, heated to the clearing temperature and cooled down to room temperature. Then, the cover plate was removed. After that the substrate with the film was again heated to clearing temperature and cooled down to

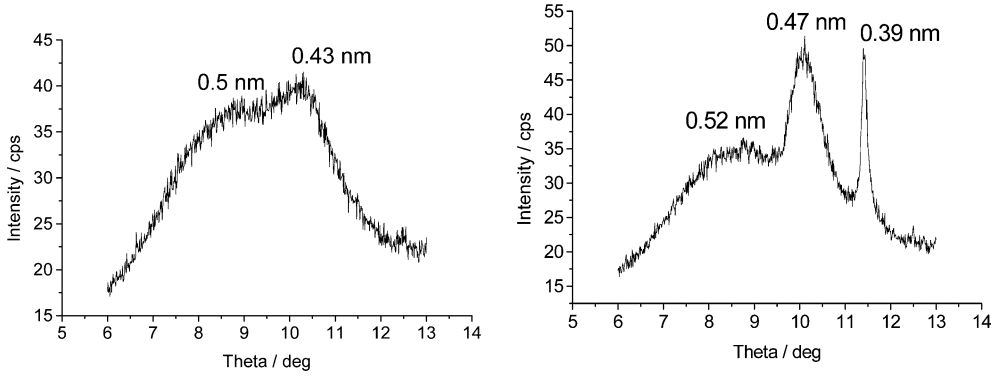

Fig. 2 **a** X-ray pattern of **P10** at 368 K (S_3). **b** X-ray pattern of **P10** at 348 K (S_4)

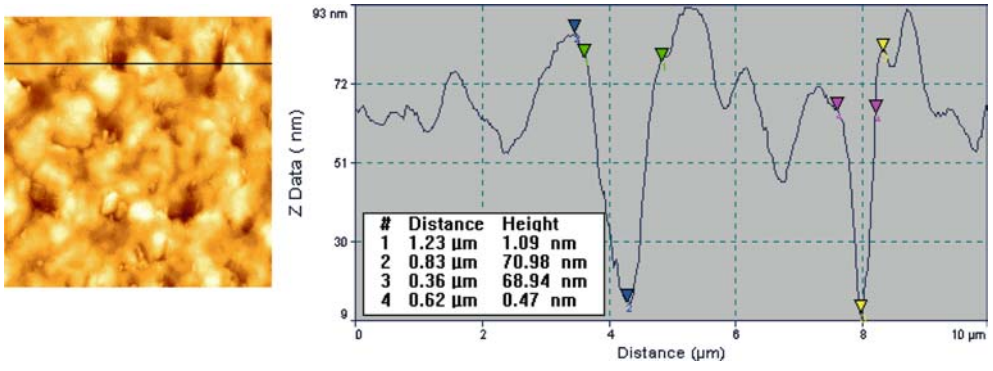

Fig. 3 AFM image of a liquid crystalline focal-conic fan texture of **P8** at 295 K. The focal conic domains are characterized by deep holes

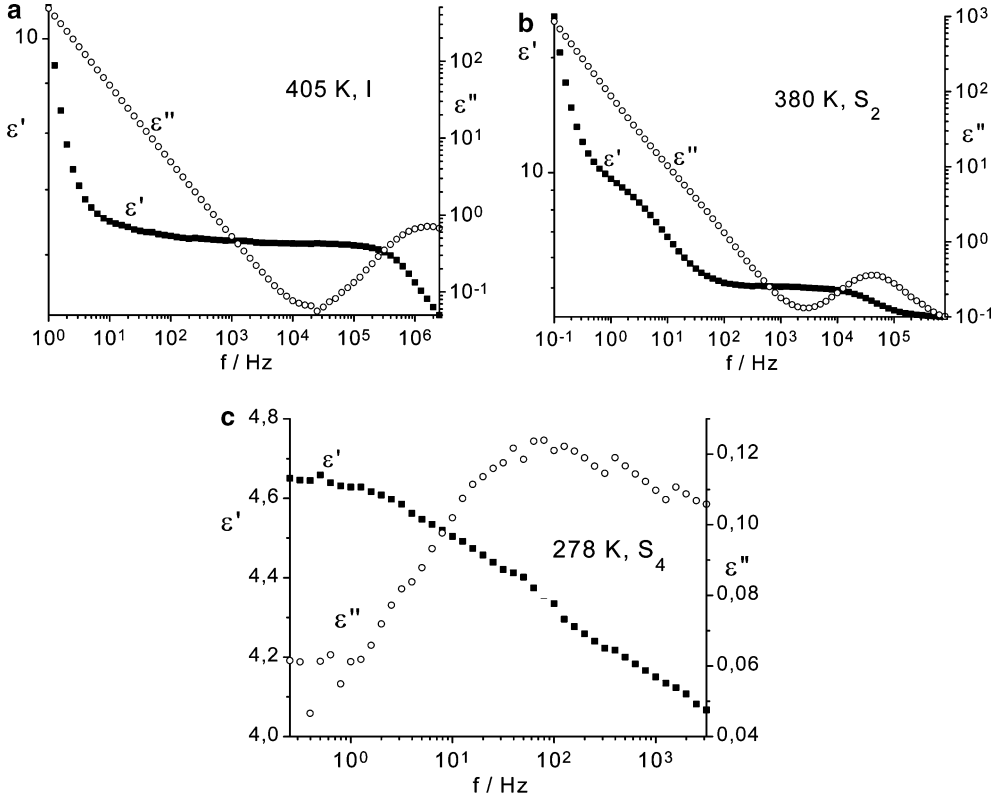

Fig. 4 **a** The complex dielectric function of **P8** in the isotropic phase. **b** The complex dielectric of **P8** in the S_2 phase. **c** The complex dielectric function of **P8** in the S_4 phase

295 K. In the cross-section of the AFM image of Fig. 4, two funnel-shaped defects are shown. The occurrence of focal-conic fan texture in the free surface of **P8** prove that the phase at 295 K is liquid crystalline characterized by a layered structure. Repeated scans at the same place results in the same surface profile. This indicates the high viscosity of the sample near to the glass transition. A phase segregation could not be seen.

Dielectric investigations

Dielectric investigations were carried out in the frequency range from 0.001 Hz to 10 MHz using the Solartron-Schlumberger Impedance Analyzer SI1260 and a Chelsea Interface. A brass cell coated with gold ($d = 0.10$ mm) was used as capacitor, which was calibrated with cyclohexane. The sample could not be oriented. The measurements were performed during stepwise cooling with a mean rate of about -0.2 Kmin^{-1}. As example, the complex dielectric function $\varepsilon^* = \varepsilon' - j\varepsilon''$ ($j^2 = -1$) of **P8** in the isotropic (I), the S_2 and the S_4 phases at low temperatures are shown in the Fig. 4a, b and c. The relaxation time of the third mechanism presented in Fig. 4c is separated by more than five decades from the second one. Therefore, all experimental points of the complex dielectric function ε^* could be fitted to Eq. (1) consisting of two COLE–COLE mechanisms [15, 16] (terms 2 and 3), a conductivity contribution (term 4) and term 5 for the description of the capacitance of the double layer at low frequencies:

$$\varepsilon^* = \varepsilon_2 + \frac{\varepsilon_S - \varepsilon_1}{1 + (j\omega\tau_1)^{1-\alpha_1}} + \frac{\varepsilon_1 - \varepsilon_2}{1 + (j\omega\tau_2)^{1-\alpha_2}} - \frac{jA}{f} + \frac{B}{f^N}, \qquad (1)$$

with ε_S—static dielectric constant, ε_i—high frequency limit of the dielectric constant, $\omega = 2\pi f$ (f—frequency), τ_i—relaxation times, α_i—Cole-Cole distribution parameters, the conductivity term A ($\kappa = 2 \cdot A \cdot \pi \cdot \varepsilon_0$, $\varepsilon_0 = 8.85 \cdot 10^{-12}$ As/Vm) as well as B and N as further fit parameters responsible for the capacity of the double layer. The third mechanism reduces the dielectric constant from ε_2 to ε_3 with the time constant τ_3. The experimental error of the data is less than 1% with exception of the very small dielectric loss shown in Fig. 4c. The error of the fitted parameter τ_i and ε_i is of 5 and 2%, respectively. This uncertainly increases to maximal 20%, if there is a strong overlapping with conductivity and double layer at low frequencies (see Fig. 4b). The error of τ_3 can reach maximal 50% due to the small intensity, overlapping with the standing wave at high frequencies and the broad distribution of this dispersion range.

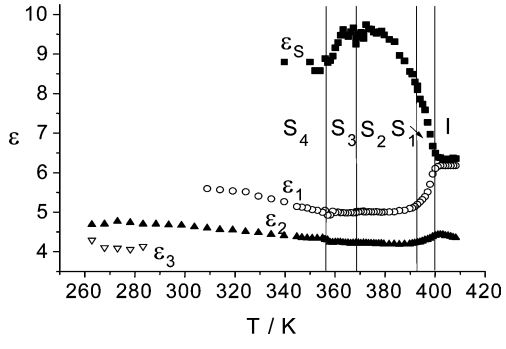

Fig. 5 Limiting values of the dielectric constants of **P8** calculated according to Eq. (1)

The results of the fits of **P8** are presented in the Figs. 5 and 6. The four limits of ε are shown in Fig. 5. The static dielectric constants ε_S increases at the transition I/S_1 indicating that the dipoles responsible for the low-frequency motion are preferably ordered parallel to the direction of the measuring electric field. The high value of the dielectric increment $\Delta\varepsilon_1 = \varepsilon_S - \varepsilon_1$ of about 4 indicates that the first process is related to the motion of the strong polar CN-dipoles. Like in other polymers, this mechanism is caused by the reorientation of the side groups around the main chain (δ-relaxation [17, 18]). This process cannot be separated below 340 K from the conductivity. It should be noted that in all phases, from I to S_4, this motion is present.

The second relaxation range reduces the dielectric constants from about 5.2 to 4.2. We interpret the related mechanism as reorientation of the main chain and parts of side group (α-process [18]). This process could be separated nearly down to room temperature. The Cole-Cole-distribution parameters of the first two

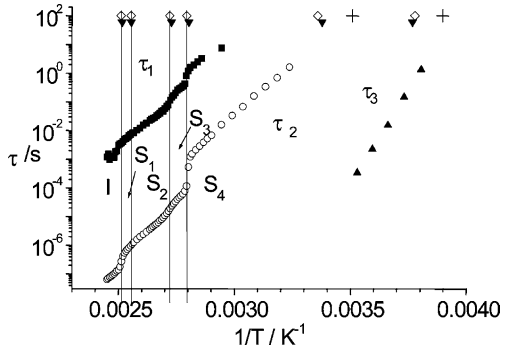

Fig. 6 ■, ○, ▲: Relaxation times of **P8** calculated using Eq. (1). The *vertical lines* indicates the phase transition temperatures seen with a heating rate of 10 K min^{-1}. The data of the TMDSC and enthalpy relaxation are included: ▼ TMDSC, maxima of for a heating run after cooling with 10 K min^{-1} ($t_p = 60$ s, $T_a = 0.4$ K, underlying heating rate $q = 2$ Kmin^{-1}), ◇ standard DSC, maxima of peaks and halfsteps, respectively for a heating run with 10 Kmin^{-1} after cooling with 10 Kmin^{-1}. + Maxima from gaussian fit of the enthalpy relaxation experiments as shown in Fig. 12B. DSC-results are given for $\tau = 100$ s

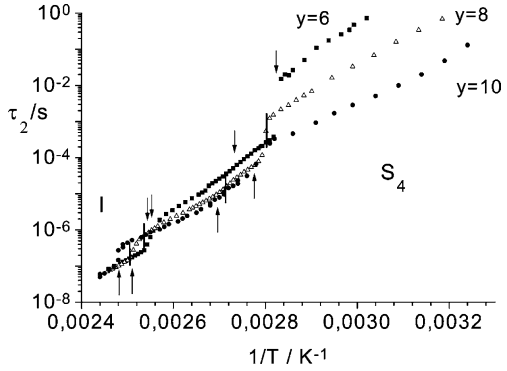

Fig. 7 Relaxation times of the α-relaxation for the three polymers. Phase transitions are indicated by ↓ for **P6**, | for **P8** and ↑ for **P10**

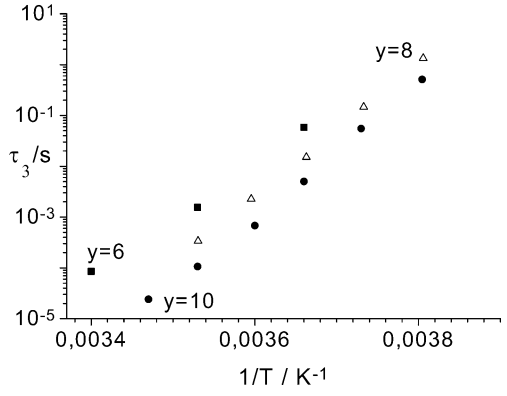

Fig. 8 Relaxation times τ_3 of the three polymers with different spacer length measured in the S_4 phase below room temperature

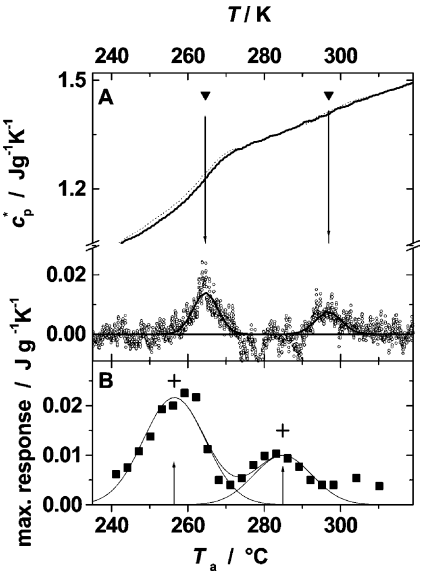

Fig. 9 **a** Sample: **P8**. Standard-DSC heat scan with 10 K/min after a cooling run with 10 K/min (*dotted line*), real part c_p' (*thick line*) and imaginary part c_p'' (°) from TMDSC with a period $t_p = 60$ s, temperature amplitude $T_a = 0.4$ K and underlying heating rate $q = 2$ K/min in the glass transition region. Maxima from the gaussian fit from c_p'' are indicated by ▼ and are the same as in Fig. 6 **b** Response from enthalpy relaxation experiments with an annealing time of 10 min for a set of temperatures T_a. ↑ peak height for the relaxation peaks, for details see text. The *crosses* (+) are the maximum from gaussian fit and are the same as in Fig. 6

mechanisms did not differ strongly ($\alpha_1 = 0.21 \pm 0.04$, $\alpha_2 = 0.15 \pm 0.05$).

The third mechanism with $\alpha_3 = 0.65 \pm 0.1$ observed only at low temperatures reduces the dielectric constants to about four. Due to the small intensity and the broad distribution, all data related to the third mechanism show an error in the relaxation time of 30%. The high activation energy of about 240 kJmol^{-1} permits to discuss this process as local dynamics.

The relaxation times are shown in Fig. 6. The first and the second mechanism are sensitive to the phase transitions found by calorimetric measurements. The following conclusions can be made by comparison of the low frequency δ-relaxation (τ_1) with known data of low-temperature liquid crystals [19]: A change of τ_1 at the S_1/S_2 transition cannot be seen. This is in accordance with the proposed SmA/SmC transition. At the S_3/S_4 transition, a stepwise increase of the relaxation time is observed. In combination with the above discussed change of the line shape of the X-ray pattern the S_4 phase may be regarded as a "solid-like" liquid crystalline phase.

The relaxation times of the α-process (τ_2, dynamics of the main chain) are for all samples sensitive to phase transitions as demonstrated in Fig. 7. Specially, this is seen for samples with a shorter spacer. Thus, for the sample with a hexyl spacer ($y = 6$) the step of τ_2 at the S_3/S_4-transition is of a factor of 20, for that with the octyl spacer of 10 and for $y = 10$ of about 2. The strong increase of the relaxation time τ_2, for the main chain at the S_3/S_4 transition may be related to the formation of a herring bone order of the side groups. Furthermore, the activation energies in the S_4 phase decreases from about 175 kJmol^{-1} ($y = 6$) to 145 kJmol^{-1} and 115 kJmol^{-1} ($y = 10$). Both, the decreasing steps and activation energy of the α-relaxation for the main chain presented in Fig. 7 may reflect the increasing de-coupling of the side group from the main chain by elongation of the spacer.

Figure 8 shows the τ_3-values related to the reorientation of the whole side groups about the own long axes [10, 11]. Like in Fig. 8a systematic increase of the relaxation times with decreasing spacer length is seen as an effect, which is also connected with the coupling between main chain and side groups.

The systematic change of the time constants τ_2 and τ_3 with variation of the spacer length makes it sure that also the related glass temperatures changes systematically. Therefore, in the following calorimetric investigations only sample **P8** was investigated in detail.

DSC-investigations, enthalpy relaxation measurements

A DSC 7 instrument (Perkin-Elmer) with TMDSC (time modulated DSC) software option was used for calorimetric measurements. The results of standard-DSC and TMDSC measurements on **P8** are presented in Fig. 9a. We found two glass transitions: the first at $T_g^{(3)} \approx 260\,K$ connected with a step in the specific heat capacity of Δc_p about 0.1 $Jg^{-1}K^{-1}$ and a peak in c_p'' and the second at $T_g^{(2)} \approx 295\,K$ characterized by $\Delta c_p \approx 0.02\,Jg^{-1}K^{-1}$ and a small reproducible and clearly detectable peak in c_p''. In both cases, the calorimetric data correlate well with the results from the dielectric relaxation processes τ_3 and τ_2 as demonstrated in Fig. 6. Therefore, also the molecular mechanism of the glass forming process can be deduced.

Enthalpy relaxation experiments can additionally confirm the existence of glass transitions. At first the sample **P8** was heated to 350 K, cooled to 220 K (rate 10 K/min) and after that again heated with a rate of 10 K/min^{-1} . In the next experiments, the sample was cooled with a rate of 10 K/min from 350 K to an annealing temperature T_a. After the annealing time $t_a = 10$ min the sample was cooled to 220 K in the glassy state and reheated with 10 K/min. The maximum of the c_p-difference between the heating curves for different T_a and that run without annealing is the maximal response shown in Fig. 9b. A plot of these maximal responses versus T_a results in a curve with a maximum at the temperature T_{max}. Usually, the highest response of this enthalpy relaxation can be observed at the temperature T_{max} is about T_g [12, 13]. The detected two local maximums for the enthalpy response in Fig. 9b are in good agreement with to the two glass transition temperatures $T^{(2)}$ and $T_g^{(3)}$ and confirm so the existence of two different glass transition. It should be pointed out that in case of **P8**, the two peaks can be well seen in contradiction to our data obtained in ref. [10, 11], where separation by computer was necessary. Thus, dielectric and calorimetric measurements as dynamical methods and the X-ray investigations give strong arguments for the existence of phase separation on the nanometer scale. The glass transition at higher temperatures is related to the freezing in of the main chain (α-relaxation) and that at lower to the rotation of the side groups about its long axis. The presented results show that main chain and liquid crystalline side groups are ordered in different phases. This principle seems to be a more common feature as expected till now.

Conclusions

Three homopolymers consisting of a tin-containing main chain and a liquid crystalline side group were characterized by different "static" and dynamic methods. It has to be pointed out that the separated side groups and main chains are miscible with each other. X-ray measurements show separated pattern of the main chains and side groups, thus that a phase separation on nanometer scale can be expected. The existence of two glass temperatures is proven by time modulated DSC measurements. Dielectric investigations did allow to relate these glass transitions to the dynamics of the phase separated main chains and side groups, respectively. Similar behavior was observed for all substances investigated. The presented results confirm a new type of phase separation induced by different order of the separated units.

Acknowledgement The authors are indebted to the DFG, Sonderforschungsbereich 418 for financial support.

Appendix

Supplement to the synthetic part

Polyesters were purified by repeated precipitation in acetone and dried in vacuum. Molecular weights of the polyesters were determined by gel permeation chromatography (GPC) with polystyrene standards and chloroform as eluant. All polyesters as well as most of the intermediary products were characterized by elemental analysis. The molecular weights of the polyesters are summarized in Table 2, together with the results of elemental analysis. In addition, the polyesters were analyzed by NMR spectroscopy. The results are in agreement with the proposed chemical structures. Yield: 60%.

^{1}H NMR ($CDCl_3$): δ = 7.65–7.64 (*d*; 2H, arom.), 7.54–7.52 (*d*; 2H, arom.), 7.44 (*d*; 2H, arom.), 7.42–7.40 (*d*; 2H, arom.), 6.96–6.92 (*d*; 2H, arom.), 6.91–6.90 (*d*; 2H, arom.), 5.12–5.10 (*s*; 2H, –O–CH_2–), 4.05–4.03 (*t*; 4H, –Sn–CH_2–CH_2–CH_2–O–), 3.94–3.93 (*t*; 2H, –CH_2–CH_2–O–), 3.30 (*t*; 1H, –CH=), 1.95–1.64 (*m*; 8H, –O–CH_2–CH_2–, =CH–CH_2–CH_2–, –Sn–CH_2–CH_2–), 1.50–1.20 [*m*; (Y−3)×2H, –CH_2–], 0.74 (*t*; 4H, –Sn–CH_2–CH_2–), 0.05–0.04 (*s*; 6H, –Sn–CH_3).

Table 2 Characterization of Polyesters **PY** by GPC and elemental analysis. M_w : weight-average, M_n : number-average molecular weight. $D = M_w/M_n$

Polyester	M_w ($g \cdot mol^{-1}$)	M_n ($g \cdot mol^{-1}$)	Elemental analysis					
			Found			Calculated		
			C	H	N	C	H	N
P6 $(718.5)_n$	39,725	19,920	61.68	6.46	1.68	61.86	6.31	1.95
P8 $(746.5)_n$	42,370	22,030	62.44	6.50	1.60	62.75	6.62	1.88
P10 $(774,6)_n$	36,215	19,125	63.89	7.03	1.63	63.58	6.90	1.81

References

1. Tschierske C (1998) J Mater Chem 6:1485
2. Blunk D, Praefke K, Vill V (1998) Amphotropic liquid crystals. In: Demus D, Goodby J, Gray GW, Spiess HW, Vill V (eds) Handbook of Liquid Crystals, vol 3. Wiley-VCH, Weinheim, pp 305–392
3. Hiltrop K (1994) Lyotropic liquid crystals. In: Stegemeyer H, Guest Ed (eds) Liquid crystals. Springer, Berlin Heidelberg New York, pp 143–171
4. Westphal S, Diele S, Mädicke A, Kuschel F, Schem U, Rühlmann K, Hisgen B, Ringsdorf H (1988) Makromol Chem Rapid Commun 9:489
5. Mao G, Oberer C (1998) Block-copolymers containing liquid-crystalline segments. In: Demus D, Goodby J, Gray GW, Spiess HW, Vill V (eds) Handbook of liquid crystals, vol 3. Wiley-VCH, Weinheim, pp 66–92
6. Roslaniec Z (2000) Poly(ether-ester) block coplymers with LC segments. In: Calleja FJB, Roslaniec Z (eds) Block copolymers, Chap 17. Marcel Dekker Inc, New York
7. Diele S, Oelsner S, Kuschel F, Hisgen B, Ringsdorf H (1988) Mol Cryst Liq Cryst 155:399
8. Kuschel F, Mädicke A, Diele S, Utschik H, Hisgen B Ringsdorf H (1990) Pol Bul 23:373
9. Emmerling U, Lindau J, Diele S, Werner J, Kresse H (2000) Liq Cryst 27:629
10. Kresse H, Lindau J, Salfetnikova J, Reichert D, Pascui O, Hempel E (2005) Liq Cryst 32:213
11. Lindau J, Salfetnikova J, Kresse H, Hempel E (2002) Proc Freiburger Arbeitstagung Flüssigkristalle (March 20th–22nd), **P6**
12. Donth E (2001) The glass transition, relaxation dynamics in liquids and disordered materials. Springer, Berlin Heidelberg New York
13. Hempel E, Beiner M, Huth H, Donth E (2002) Thermochimica Acta 391:219
14. Guinier A (1956) Theorie et Technique de la Radiocristallographie. Dunod, Paris, p 196
15. Hill NE, Vaughan WE, Price AH, Davies M (1969) Dielectric properties and molecular behaviour. van Nostrand, New York, pp 49–54
16. Kremer F, Schönhals A (2003) Broadband dielectric spectroscopy. Springer, Berlin Heidelberg New York, pp 59–98
17. Kresse H, Talroze RV (1981) Macromol Chem Rapid Commun 2:369
18. Zentel R, Strobl G, Ringsdorf H (1985) Recent advances in liquid crystalline polymers. In: Chapoy LL (ed) Elsevier Applied Sciences, London
19. Kresse H (1993) Dynamics in thermotropic calamitic liquid crystals investigated by dielectric methods. In: Buka A (ed) Modern topics of liquid crystals. World Scientific, Singapore, pp 26–27